

Interfacial origin of unconventional spin-orbit torque in Py/ γ -IrMn₃

Akash Kumar,^{1,2, a)} Pankhuri Gupta,^{1, a)} Niru Chowdhury,¹ Kacho Imtiyaz Ali Khan,¹ Utkarsh Shashank,³ Surbhi Gupta,³ Yasuhiro Fukuma,³ Sujeet Chaudhary,¹ and Pranaba Kishor Muduli*¹

¹⁾Department of Physics, Indian Institute of Technology Delhi, Hauz Khas, New Delhi 110016, India.

²⁾Department of Physics, University of Gothenburg, Gothenburg, 412 96, Sweden

³⁾Department of Physics and Information Technology, Kyushu Institute of Technology, Iizuka, Fukuoka 820-8502, Japan.

(*Electronic mail: muduli@physics.iitd.ac.in)

(Dated: 9 May 2023)

Angle-resolved spin-torque ferromagnetic resonance measurements are carried out in heterostructures consisting of Py (Ni₈₁Fe₁₉) and a noncollinear antiferromagnetic quantum material γ -IrMn₃. The structural characterization reveals that γ -IrMn₃ is polycrystalline in nature. A large exchange bias of 158 Oe is found in Py/ γ -IrMn₃ at room temperature, while γ -IrMn₃/Py and Py/Cu/ γ -IrMn₃ exhibited no exchange bias. Regardless of the exchange bias and stacking sequence, we observe a substantial unconventional out-of-plane anti-damping torque when γ -IrMn₃ is in direct contact with Py. The magnitude of the out-of-plane spin-orbit torque efficiency is found to be twice as large as the in-plane spin-orbit torque efficiency. The unconventional spin-orbit torque vanishes when a Cu spacer is introduced between Py and γ -IrMn₃, indicating that the unconventional spin-orbit torque in this system originates at the interface. These findings are important for realizing efficient antiferromagnet-based spintronic devices via interfacial engineering.

Spin-orbit torques (SOTs) in ferromagnetic/heavy metal (FM/HM) heterostructures have emerged as a powerful tool for a wide range of spintronic applications.^{1–6} Large anti-damping SOTs are of utmost interest and play a pivotal role in ultrafast magnetization switching^{3,7}, spintronic oscillators^{4,6,8–10} as well as the emerging area of spintronic-based neuromorphic computing.^{11–15} In the FM/HM system, the SOT is generated either via the spin Hall effect^{16–19} from the HM layer and/or the Rashba-Edelstein effect^{20,21} from the interface between the FM and HM layers. In both cases, when a charge current flows in the x -direction, it generates a spin current in the z -direction with the spin polarization along the y -direction, which can apply an in-plane anti-damping torque on the adjacent FM layer.^{2,19} This is often referred to as “conventional SOT.” Due to the symmetry of the conventional SOT, it is difficult to achieve deterministic switching of a perpendicularly magnetized system used in high-density magnetic recording. Recently, an out-of-plane damping-like torque was reported in WTe₂/Py by using the low crystalline symmetry of WTe₂.²² Field-free switching in perpendicularly magnetized FMs using the unconventional spin-orbit torques (USOTs) in WTe₂ was also demonstrated recently.²³ Since then, USOTs have been reported in non-collinear antiferromagnets such as Mn₃GaN²⁴, Mn₃SnN²⁵, Mn₃Sn²⁶ and IrMn₃²⁷ by using their low magnetic symmetry, which gives rise to an out-of-plane spin polarization for in-plane charge currents. The non-collinear antiferromagnetic also exhibits a large anomalous Hall effect due to the non-zero Berry curvature caused by the spin texture in the Kagome plane.^{28–33} In addition, the ferromagnetic/antiferromagnetic (FM/AFM) bilayer systems are also extensively explored for the presence of exchange bias³⁴ and large SOTs, which lead to field-free switching of ferromagnets.^{35–37} Particularly, for

the non-collinear antiferromagnet IrMn₃, an unconventional torque is reported for epitaxial L1₀-IrMn and L1₂-IrMn.²⁷

In this work, we investigate SOT in Py(= Ni₈₁Fe₁₉)/ γ -IrMn₃, γ -IrMn₃/Py and Py/Cu/ γ -IrMn₃ using the spin-torque ferromagnetic resonance (STFMR) technique and determine ξ_{DL}^x , ξ_{DL}^y and ξ_{DL}^z which represents damping-like spin torque efficiency in x -, y - and z -direction, respectively. All the three components ξ_{DL}^x , ξ_{DL}^y , and ξ_{DL}^z are found to be present in Py/ γ -IrMn₃, γ -IrMn₃/Py system, while only ξ_{DL}^y is found to be present in Py/Cu/ γ -IrMn₃. This means that while USOT exists in both Py/ γ -IrMn₃ and γ -IrMn₃/Py systems, the Py/Cu/ γ -IrMn₃ system has only conventional SOT. Thus, the USOT in our case arises from the interface between Py and polycrystalline γ -IrMn₃, which is in stark contrast with previous findings where the USOT was observed only due to the presence of low magnetic symmetry in the bulk of IrMn₃.²⁷ Our results show that USOT can be obtained using a CMOS-compatible naturally oxidized high resistive Si substrate, unlike previous studies of Zhou *et al.*,²⁷ for which the authors used specialized substrates, which is not compatible with CMOS-technology.

The thin film heterostructures are grown using an AJA Orion 8 UHV magnetron sputtering system at room temperature. The base pressure of the sputtering system is better than 2×10^{-8} Torr. Samples were grown at a working pressure of 1×10^{-3} Torr. First, we optimized the growth of IrMn₃. We used a target with the composition of 20 at% Ir and 80 at% Mn. Subsequently, we deposited multilayer samples with Py and γ -IrMn₃ on Si substrates at room temperature. The structural characterization was performed using X-ray diffraction (XRD) using a PANalytical x-ray diffractometer equipped with Cu K α ($\lambda = 1.5406$ Å) source. We use in-plane grazing incidence X-ray diffraction at an incidence angle of 1° to determine the crystalline phase of IrMn, as shown in Fig. 1(a). The Bragg peaks are observed at $2\theta = 41.6^\circ, 48.3^\circ, 70.7^\circ, \text{ and } 85.4^\circ$, which correspond to the IrMn₃

^{a)}These authors contributed equally.

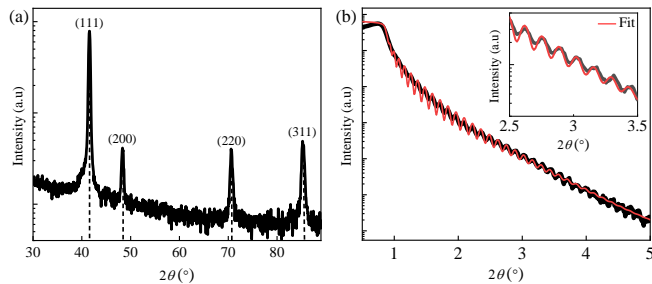


FIG. 1. (a) Grazing-incidence X-ray diffraction spectrum measured in $\theta - 2\theta$ mode, and (b) X-ray reflectivity spectra (black line) as well as the fit (red line) for a 62 nm thick IrMn₃ thin film. The inset in (b) shows a zoomed portion of XRR spectra with the fit (red line).

(111), (200), and (220) and (311)-planes, respectively. The superlattice reflection of L1₂-IrMn₃, namely peaks corresponding to (110) and (211), are absent in our sample, indicating polycrystalline growth of only γ -IrMn₃ phase.^{38,39} The thickness, density, and roughness of the films were analyzed using X-ray reflectivity (XRR) technique and fitted using recursive Parratt's formalism⁴⁰ as shown in Fig. 1(b). The thickness and roughness of γ -IrMn₃ in this thin film were found to be ≈ 62 nm and < 0.3 nm, respectively. The optimal growth rate of γ -IrMn₃ was ≈ 0.9 Å/s. The zoomed XRR spectrum and respective fit are shown in the inset of Fig. 1(b). From the XRR measurements, the interface roughness of multilayer structures was found to be < 0.3 nm (not shown). To induce exchange bias, these structures were grown in the presence of a 300 Oe *in-situ* in-plane magnetic field. To avoid oxidation, samples were capped with 2 nm Ta or Pt thin films. Microstrip devices of dimension ($4 \mu\text{m} \times 12 \mu\text{m}$) were fabricated for the STFMR measurements using optical lithography followed by Ar-ion etching. Ground-signal-ground electrodes with 150 μm pitch are fabricated for contact pads. In the present manuscript, we discuss the results for three samples, denoted by Py/ γ -IrMn₃: Py (8.7 nm)/ γ -IrMn₃(13 nm), γ -IrMn₃/Py: γ -IrMn₃(15 nm)/Py(20 nm), and Py/Cu/ γ -IrMn₃: Py(10 nm)/Cu(1.5 nm)/ γ -IrMn₃(13 nm).

Figure 2 shows the magneto-optic Kerr effect (MOKE) measurements performed in the longitudinal configuration with an intensity stabilized He-Ne laser (5 mW and wavelength of 632.8 nm). The incident laser light was *p*-polarized, and the reflected light is passed through a photoelastic modulator (PEM) followed by an analyzer kept at 45° with respect to the first polarizer. A photodiode was then used to measure the MOKE signal using the lock-in technique. The lock-in amplifier was locked to the second harmonic of PEM frequency. More details of the MOKE setup can be found elsewhere.⁴¹ Figure 2(a), (b), and (c) shows the hysteresis loops measured using the magneto-optic Kerr effect at room temperature for Py/ γ -IrMn₃, γ -IrMn₃/Py and Py/Cu/ γ -IrMn₃ samples, respectively. The sample Py/ γ -IrMn₃ in which γ -IrMn₃ is deposited on top of Py shows large exchange bias, H_{ex} of about 158 Oe. However, we do not observe any exchange bias in samples with reversed stack sequence⁴², *i.e.*, γ -IrMn₃/Py as well as in the sample with Cu spacer

i.e., Py/Cu/ γ -IrMn₃. We use 1.5 nm thick Cu spacer to break any interfacial coupling between Py and γ -IrMn₃, as shown in Supplementary Fig. S1. Microstrip devices of dimension ($4 \mu\text{m} \times 12 \mu\text{m}$) were fabricated for the STFMR measurements. For the STFMR measurements, a bias tee is utilized to separate the DC (rectified voltage) and RF port (high-frequency RF current) connected to the microstrip via a Ground-signal-Ground probe.⁴³ The high-frequency RF current was supplied by R&S signal generator (SMB 100A) at a constant RF power of +3 dBm. The RF signal was amplitude modulated with an 86 Hz signal. The rectified voltage V_{DC} was detected using a lock-in amplifier. The magnetic field was applied in the sample plane at an angle ϕ with respect to the current direction (*x*-direction) along the long axis of the microstrip. The angle, ϕ , was varied from (0 – 360°) with the help of a vector field magnet. Figure 2(c), (d) and (e) show examples of STFMR spectra measured at 8 GHz with $\phi = 60^\circ$ for Py/ γ -IrMn₃, γ -IrMn₃/Py and Py/Cu/ γ -IrMn₃, respectively. Due to the presence of exchange bias, the resonance field (H_R) for the positive and negative fields was found to be different only for Py/ γ -IrMn₃. We determine the exchange bias as $H_{ex} = |H_R(H > 0) - H_R(H < 0)|/2$ and found it to be 80 Oe (at $\phi = 60^\circ$), which agrees with the magneto-optic Kerr effect measurements after taking into account of the angular dependence of exchange bias. The lineshape of measured STFMR spectra for the three devices shows dramatically different behavior. For both Py/ γ -IrMn₃ and γ -IrMn₃/Py, the lineshape is found to change upon reversal of the field polarity. However, no such change of lineshape with field polarity is observed for Py/Cu/ γ -IrMn₃, which is similar to the case of the FM/HM system.^{22,44} The measured STFMR signal (V_{DC}) can be fitted using a combination of symmetric and anti-symmetric Lorentzian function^{43,44}:

$$V_{DC} = V_S \frac{\Delta H^2}{\Delta H^2 + (H - H_R)^2} + V_A \frac{\Delta H(H - H_R)}{\Delta H^2 + (H - H_R)^2}, \quad (1)$$

Where V_S and V_A are symmetric and anti-symmetric voltage components of the rectified voltage. ΔH represents the linewidth. The measured STFMR data are fitted with the above equation, as shown by solid lines. We also separately show the symmetric (black) and antisymmetric (red) components.

The magnitude and/or sign of V_S and V_A are found to change with the reversal of field polarity for Py/ γ -IrMn₃ and γ -IrMn₃/Py. For a conventional SOT, only sign of V_S and V_A should change with the reversal of field polarity. Hence, the SOT for Py/ γ -IrMn₃ and γ -IrMn₃/Py can be considered unconventional. However, when the 1.5 nm thick Cu spacer is present between Py and γ -IrMn₃, only sign of V_S and V_A changes with the reversal of field polarity- indicating the absence of USOT. Thus, these results indicate that the USOT in our system does not arise from the bulk γ -IrMn₃ but from the interface of Py and γ -IrMn₃. This is in stark contrast to the recent results of USOT in L1₂-IrMn₃/Py by Zhou *et al.*²⁷, where the USOT was present even with the insertion of Cu layer. Moreover, Zhou *et al.* used epitaxial L1₂-IrMn₃, whereas we have γ -IrMn₃ phase, for which no

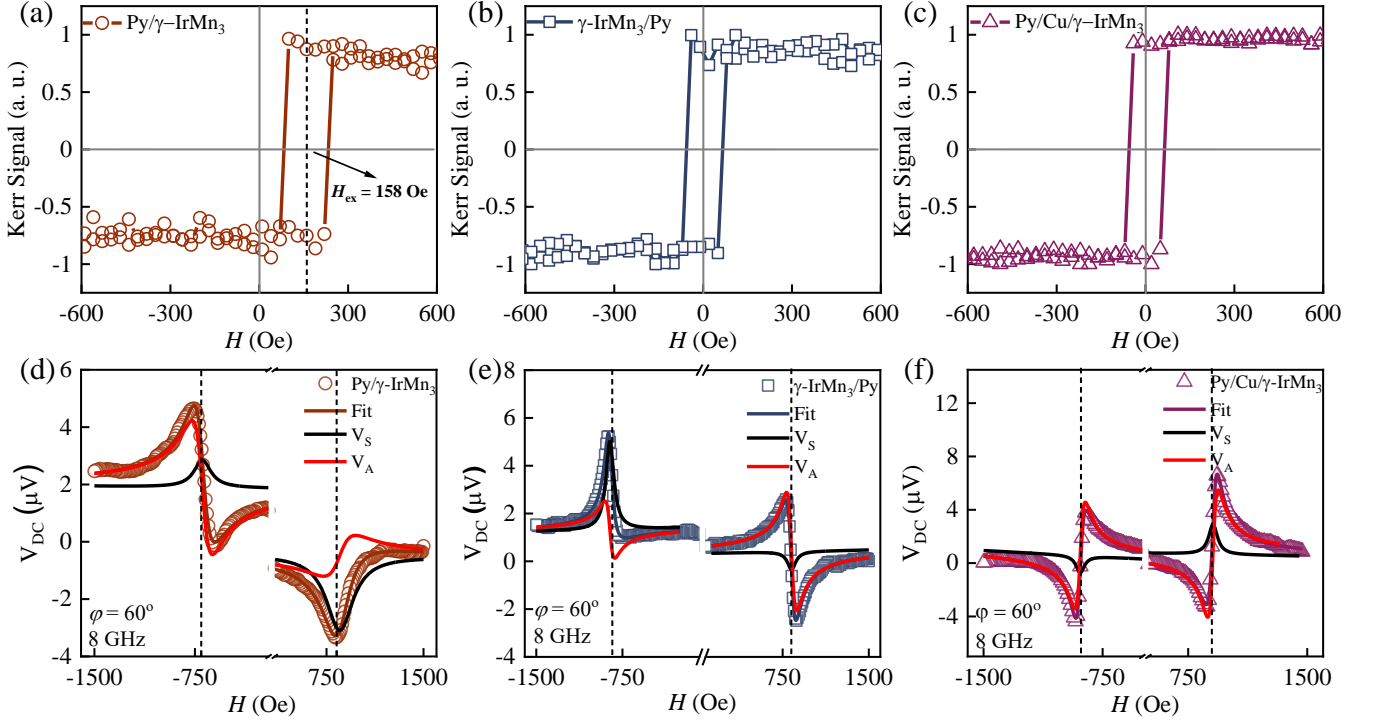


FIG. 2. Magnetic hysteresis loops measured using magneto-optic Kerr effect magnetometer for (a) Py/ γ -IrMn₃, (b) γ -IrMn₃/Py, and (c) Py/Cu/ γ -IrMn₃, respectively. A positive exchange bias of 158 Oe was observed for the sample with γ -IrMn₃ grown directly on top of Py. STFM measurement for (d) Py/ γ -IrMn₃, (e) γ -IrMn₃/Py, and (f) Py/Cu/ γ -IrMn₃, respectively. The solid line is the Lorentzian fit using Eq 1. The symmetric (V_S) and anti-symmetric (V_A) components of the fitted curve are depicted in black and red, respectively. The STFM measurements reveal that Py/ γ -IrMn₃ and γ -IrMn₃/Py systems show a dramatic change of lineshape with field reversal, which is absent in the Py/Cu/ γ -IrMn₃ system.

USOT is expected from the broken magnetic mirror symmetry.²⁷ Additionally, any USOT due to bulk crystal structure is expected to be averaged out for polycrystalline films. Furthermore, USOTs are present even without the exchange bias for γ -IrMn₃/Py indicating that USOT, which we observe, is not linked to the exchange bias.

To systematically examine the presence of USOT and quantify the damping-like torque efficiencies, we have performed complete angular dependent STFM measurements as shown in Fig. 3. First, second and third column corresponds to Py/ γ -IrMn₃, γ -IrMn₃/Py and Py/Cu/ γ -IrMn₃, respectively. Figure 3(a), (b), and (c) show the extracted symmetric voltage components, and Fig. 3(d), (e), and (f) show the extracted anti-symmetric voltage components. Conventional SOTs (spin polarization along the y -direction) lead to $\sin(2\varphi)\cos(\varphi)$ -dependence for both symmetric and anti-symmetric voltage components.^{22,45} However, the data for Py/ γ -IrMn₃ and γ -IrMn₃/Py do not follow the $\sin(2\varphi)\cos(\varphi)$ -dependence indicating that the spin polarization is not restricted to the y -direction only but also have x - and z - components. Considering the spin polarization in an arbitrary direction, the angular dependence of V_S and V_A components can be generalized as^{22,24,45}:

$$V_S = S_{DL}^x \sin(2\varphi) \sin(\varphi) + S_{DL}^y \sin(2\varphi) \cos(\varphi) + S_{FL}^z \sin(2\varphi) \quad (2)$$

$$V_A = A_{FL}^x \sin(2\varphi) \sin(\varphi) + A_{FL}^y \sin(2\varphi) \cos(\varphi) + A_{DL}^z \sin(2\varphi). \quad (3)$$

Here, S_{DL}^x , S_{DL}^y and A_{DL}^z are the coefficients for the damping-like torque generated by the different components of spin Hall conductivity tensor, σ_{zx}^x , σ_{zx}^y , and σ_{zx}^z respectively. Similarly, A_{FL}^x , A_{FL}^y , and S_{FL}^z represent the coefficients corresponding to a field-like component of the spin Hall conductivity tensor. Thus by fitting the angular dependence of V_S and V_A using Eq. 2 and Eq. 3, various contributions can be separated. Assuming that A_{FL}^y is due to the Oersted field alone, we can quantify the amplitude of three components of damping-like torque efficiencies.^{27,45}

$$\xi_{DL}^x = \frac{S_{DL}^x}{A_{FL}^y} \frac{e\mu_0 M_S t_{FM} d_{NM}}{\hbar} \left[1 + \frac{4\pi M_{eff}}{H_R} \right]^{1/2} \quad (4)$$

$$\xi_{DL}^y = \frac{S_{DL}^y}{A_{FL}^y} \frac{e\mu_0 M_S t_{FM} d_{NM}}{\hbar} \left[1 + \frac{4\pi M_{eff}}{H_R} \right]^{1/2} \quad (5)$$

$$\xi_{DL}^z = \frac{A_{DL}^z}{A_{FL}^y} \frac{e\mu_0 M_S t_{FM} d_{NM}}{\hbar} \quad (6)$$

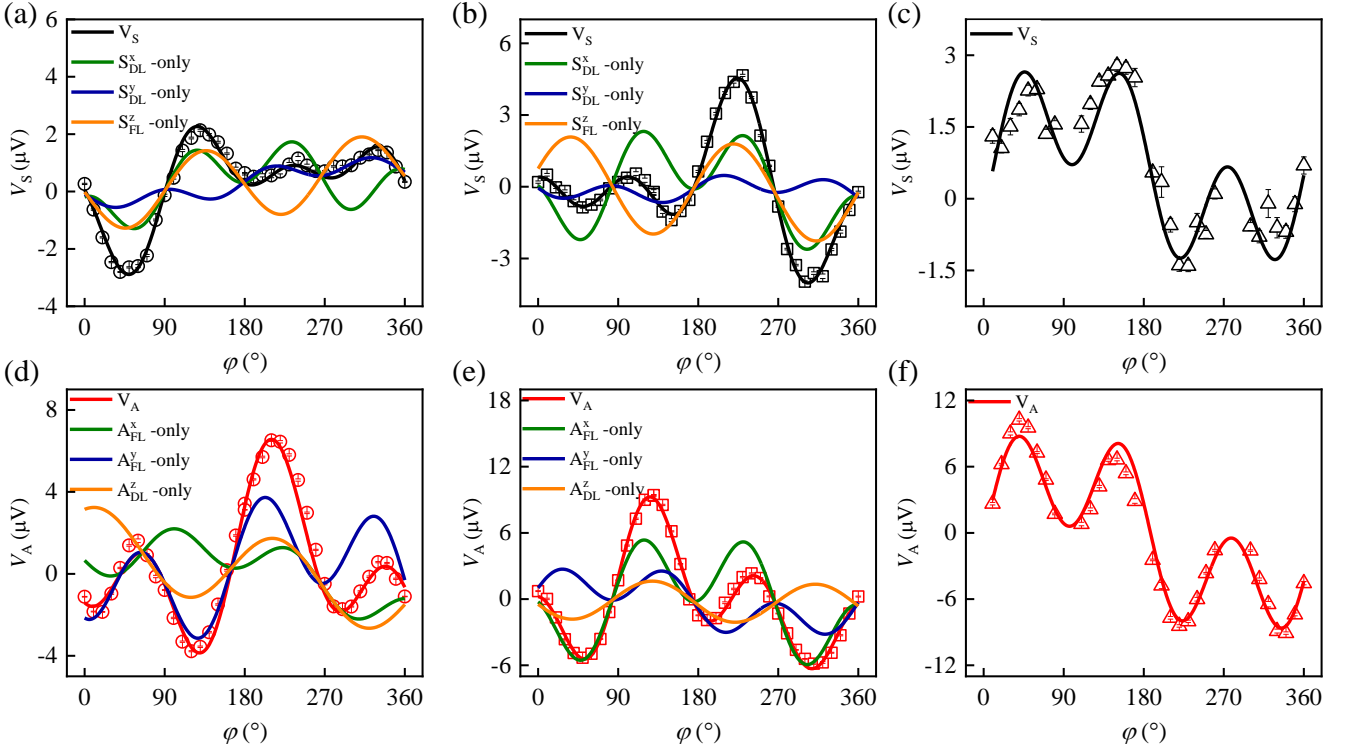


FIG. 3. Angular dependence of V_S and V_A components for (a), and (d) Py/ γ -IrMn₃, (b), and (e) γ -IrMn₃/Py (c), and (f) Py/Cu/ γ -IrMn₃ sample with Cu spacer to avoid exchange coupling between Py and γ -IrMn₃. The fitting (solid lines) is performed using Eq. 2 and Eq. 3. The other solid lines (brown, blue, and green) show the extracted angular dependence of voltage contributions from x -, y -, and z -direction spin polarization.

Here, d_{NM} and t_{FM} are the non-magnetic and ferromagnetic layer thicknesses, respectively. The parameters e , \hbar , and M_S represent the electric charge, reduced Planck's constant, and saturation magnetization, respectively. The effective magnetization, M_{eff} , is determined from the fitting of f versus H_R [obtained from Eq. 1] data using the Kittel equation.⁴⁶

Table S1 summarizes the results of fitting of angular dependence of V_S and V_A for Py/ γ -IrMn₃, γ -IrMn₃/Py and Py/Cu/ γ -IrMn₃ structure. In the table, ξ_{DL}^y denotes the effective conventional damping-like efficiency in the y -direction, while ξ_{DL}^x and ξ_{DL}^z represent the unconventional damping-like efficiencies in the x - and z -direction, respectively. All the three components ξ_{DL}^y , ξ_{DL}^x , and ξ_{DL}^z are found to be present in Py/ γ -IrMn₃, γ -IrMn₃/Py system, while only ξ_{DL}^y is found to be present in Py/Cu/ γ -IrMn₃. The conventional damping-like efficiency ξ_{DL}^y is found to be (0.08 ± 0.03) , (-0.25 ± 0.02) and (0.16 ± 0.02) for Py/ γ -IrMn₃, γ -IrMn₃/Py and Py/Cu/ γ -IrMn₃, respectively. Here, the sign change in amplitude for ξ_{DL}^y for Py/ γ -IrMn₃, γ -IrMn₃/Py is observed because of the stack sequence. The uncertainty in damping-like efficiency values denotes device-to-device variability and fitting errors in V_S and V_A . The magnitude of ξ_{DL}^y for Py/Cu/ γ -IrMn₃ is found to be greater than that of Py/ γ -IrMn₃ and lower than that of γ -IrMn₃/Py system. This implies that the unconventional contributions in Py/ γ -IrMn₃ and γ -IrMn₃/Py directly increase or decrease the bulk ξ_{DL}^y resulting in higher or lower effective ξ_{DL}^y . In an earlier re-

port by Tshitoyan, *et al.*⁴⁷, ξ_{DL}^y was reported to be higher for Py/IrMn compared to Py/Cu/IrMn, which was correlated to the exchange bias. In contrast, our study shows a higher value of the ξ_{DL}^y for Py/Cu/ γ -IrMn₃ compared to the exchange biased sample Py/ γ -IrMn₃ indicating a different mechanism of damping-like spin-orbit torque in our system. We believe this is due to a combination of bulk and interfacial effects.⁴⁸ The bulk effect from γ -IrMn₃ can be considered as the value of ξ_{DL}^y we measure for Py/Cu/ γ -IrMn₃. The interfacial contributions for Py/ γ -IrMn₃ and γ -IrMn₃/Py have opposite signs, which explains the observed values of ξ_{DL}^y .

The unconventional efficiencies in our system are of pure interfacial origin, as stated earlier. The x - component of USOT (ξ_{DL}^x) is found to be 0.28 ± 0.04 and 0.55 ± 0.07 for Py/ γ -IrMn₃ and γ -IrMn₃/Py, respectively. Similarly, the z - component of USOT (ξ_{DL}^z) is found to be -0.12 ± 0.02 and -0.40 ± 0.11 for Py/ γ -IrMn₃ and γ -IrMn₃/Py, respectively. Interestingly, unconventional torque efficiencies are larger than conventional ξ_{DL}^y , which has never been reported before to our knowledge. We also investigated the dependency of USOT on the thickness of Py layer. We do not observe any systematic variation of USOT with Py thickness, as shown in Supplementary Fig. S2. However, we consistently find that the unconventional torque efficiencies are larger than the conventional ξ_{DL}^y for a different devices and with varying Py thicknesses.

We believe the generation of USOTs at the interface of Py

TABLE I. Exchange bias, damping-like efficiency, and spin polarization for Py/ γ -IrMn₃, γ -IrMn₃/Py and Py/Cu/ γ -IrMn₃.

Sample	Exchange Bias (Oe)	Direction of polarization	Damping-like efficiency		
			ξ_{DL}^x	ξ_{DL}^y	ξ_{DL}^z
Py/ γ -IrMn ₃	158 Oe	x -, y -, and z - direction	0.28 \pm 0.04	0.08 \pm 0.03	-0.12 \pm 0.02
γ -IrMn ₃ /Py	0 Oe	x -, y -, and z - direction	0.55 \pm 0.07	-0.25 \pm 0.03	-0.40 \pm 0.11
Py/Cu/ γ -IrMn ₃	0 Oe	y - direction only	0	0.16 \pm 0.02	0

and γ -IrMn₃ could be due to the spin swapping effect⁴⁹. The Py/ γ -IrMn₃ interface works as a magnetic scattering center causing spin swapping (exchange of spin polarization and flow) of bulk spin currents generated by the interior of γ -IrMn₃. The interfacial scattering can deflect the spin current flow, resulting in the generation of spin currents polarized in x - and z - directions, which are non-trivial in nature for normal heavy metals exhibiting the bulk spin Hall effect.¹⁹ A similar effect was recently observed in another collinear antiferromagnet, Mn₃Sn.⁵⁰ Hence, we believe the interfacial USOT that we observe is unique to γ -IrMn₃, since such USOT has not been reported in IrMn previously.^{47,51,52}

We observed unconventional spin-orbit torques in heterostructures consisting of Py and polycrystalline γ -IrMn₃. The systematic investigation of the angular dependence of symmetric and anti-symmetric components of STFM measurements suggests the presence of unconventional spin-orbit torques in Py/ γ -IrMn₃ and γ -IrMn₃/Py. The interface between Py and γ -IrMn₃ gives rise to substantial out-of-plane damping-like spin-orbit torques in addition to the conventional spin-orbit torques. These unconventional spin-orbit torques can be eliminated by inserting a Cu spacer between Py and γ -IrMn₃-indicating an interfacial origin of the unconventional spin-orbit torques in contrast to the previously reported studies that demonstrated a bulk origin arising from the magnetic mirror asymmetry in IrMn₃. A large in-plane damping-like efficiency of 0.16 is also observed for the Py/Cu/ γ -IrMn₃ system, indicating that γ -IrMn₃ is an efficient source of spin current. These findings emphasize the importance of investigating the interfacial origin of these torques to comprehend the physics of collinear antiferromagnets. The large out-of-plane damping-like efficiency that we observed in our system can be utilized to effectively switch a perpendicularly magnetized system used in high-density magnetic recording.^{3,36} Therefore, it has high technological relevance for energy-efficient spintronic devices based on quantum materials.

ACKNOWLEDGMENTS

We acknowledge the Department of Science and Technology for supporting this collaborative work under the Indo-Japan project (grant no: *DST/INT/JSPP/P* – 266/2018). The partial support from the Science & Engineering Research Board (SERB File no. CRG/2018/001012), the Ministry of Human Resource Development under the IMPRINT program (Grant no: 7519 and 7058), the Department of Science and Technology under the Nanomission program (grant no: *SR/NM/NT* – 1041/2016(*G*)), the Department of Electronics and Information Technology (DeitY), Joint Advanced

Technology Centre at IIT Delhi, and the Grand Challenge project supported by IIT Delhi are gratefully acknowledged. A. K. acknowledges support from the Council of Scientific and Industrial Research (CSIR), India.

I. AUTHOR DECLARATIONS

Conflict of Interest

The authors have no conflicts to disclose.

II. DATA AVAILABILITY

The data that support the findings of this study are available from the corresponding author upon reasonable request.

- ¹K. Ando, S. Takahashi, K. Harii, K. Sasage, J. Ieda, S. Maekawa, and E. Saitoh, *Phys. Rev. Lett.* **101**, 036601 (2008).
- ²P. Gambardella and I. M. Miron, *Proc. Natl. Acad. Sci.* **369**, 3175 (2011).
- ³L. Liu, C.-F. Pai, Y. Li, H. W. Tseng, D. C. Ralph, and R. A. Buhrman, *Science* **336**, 555 (2012).
- ⁴V. E. Demidov, S. Urazhdin, H. Ulrichs, V. Tiberkevich, A. Slavin, D. Baither, G. Schmitz, and S. O. Demokritov, *Nat. Mater.* **11**, 1028 (2012).
- ⁵S. Emori, U. Bauer, S.-M. Ahn, E. Martinez, and G. S. D. Beach, *Nat. Mater.* **12**, 611 (2013).
- ⁶A. A. Awad, P. Dürrenfeld, A. Houshang, M. Dvornik, E. Iacocca, R. K. Dumas, and J. Åkerman, *Nat. Phys.* **13**, 292 (2016).
- ⁷K. Garello, C. O. Avci, I. M. Miron, M. Baumgartner, A. Ghosh, S. Auffret, O. Boulle, G. Gaudin, and P. Gambardella, *Appl. Phys. Lett.* **105**, 212402 (2014).
- ⁸T. Chen, R. K. Dumas, A. Eklund, P. K. Muduli, A. Houshang, A. A. Awad, P. Dürrenfeld, B. G. Malm, A. Rusu, and J. Åkerman, *Proc. IEEE* **104**, 1919 (2016).
- ⁹N. Behera, H. Fulara, L. Bainsla, A. Kumar, M. Zahedinejad, A. Houshang, and J. Åkerman, *Phys. Rev. Appl.* **18**, 024017 (2022).
- ¹⁰A. Kumar, H. Fulara, R. Khymyn, M. Zahedinejad, M. Rajabali, X. Zhao, N. Behera, A. Houshang, A. A. Awad, and J. Åkerman, *arXiv* **2301.03859** (2023).
- ¹¹M. Zahedinejad, A. A. Awad, S. Muralidhar, R. Khymyn, H. Fulara, H. Mazraati, M. Dvornik, and J. Åkerman, *Nat. Nano.* **15**, 47 (2020).
- ¹²A. Houshang, M. Zahedinejad, S. Muralidhar, R. Khymyn, M. Rajabali, H. Fulara, A. A. Awad, J. Åkerman, J. Cechiński, and M. Dvornik, *Phys. Rev. Appl.* **17**, 014003 (2022).
- ¹³N. Garg, S. V. H. Bhotla, P. K. Muduli, and D. Bhowmik, *Neuromorph. Comput. Eng.* **1**, 024005 (2021).
- ¹⁴A. Kumar, M. Rajabali, V. H. González, M. Zahedinejad, A. Houshang, and J. Åkerman, *Nanoscale* **14**, 1432 (2022).
- ¹⁵R. S. Yadav, P. Gupta, A. Holla, K. I. Ali Khan, P. K. Muduli, and D. Bhowmik, *ACS Appl. Electron. Mater.* **5**, 484 (2023).
- ¹⁶M. I. Dyakonov and V. I. Perel, *Phys. Lett. A* **35**, 459 (1971).
- ¹⁷J. E. Hirsch, *Phys. Rev. Lett.* **83**, 1834 (1999).
- ¹⁸J. Sinova, S. O. Valenzuela, J. Wunderlich, C. H. Back, and T. Jungwirth, *Rev. Mod. Phys.* **87**, 1213 (2015).

- ¹⁹A. Manchon, J. Železný, I. M. Miron, T. Jungwirth, J. Sinova, A. Thiaville, K. Garello, and P. Gambardella, *Rev. Mod. Phys.* **91**, 035004 (2019).
- ²⁰Y. A. Bychkov and É. I. Rashba, *JETP Lett.* **39**, 78 (1984).
- ²¹V. M. Edelstein, *Solid State Commun.* **73**, 233 (1990).
- ²²D. MacNeill, G. M. Stiehl, M. H. D. Guimarães, R. A. Buhrman, J. Park, and D. C. Ralph, *Nat. Phys.* **13**, 300 (2017).
- ²³Q. Xie, W. Lin, S. Sarkar, X. Shu, S. Chen, L. Liu, T. Zhao, C. Zhou, H. Wang, J. Zhou, S. Gradečák, and J. Chen, *APL Mater.* **9**, 051114 (2021).
- ²⁴T. Nan, C. X. Quintela, J. Irwin, G. Gurung, D. F. Shao, J. Gibbons, N. Campbell, K. Song, S. Y. Choi, L. Guo, R. D. Johnson, P. Manuel, R. V. Chopdekar, I. Hallsteinsen, T. Tybell, P. J. Ryan, J. W. Kim, Y. Choi, P. G. Radaelli, D. C. Ralph, E. Y. Tsymbal, M. S. Rzechowski, and C. B. Eom, *Nat. Commun.* **11**, 1 (2020).
- ²⁵Y. You, H. Bai, X. Feng, X. Fan, L. Han, X. Zhou, Y. Zhou, R. Zhang, T. Chen, F. Pan, and C. Song, *Nat. Commun.* **12**, 1 (2021).
- ²⁶K. Kondou, H. Chen, T. Tomita, M. Ikhlas, T. Higo, A. H. MacDonald, S. Nakatsuji, and Y. Otani, *Nat. Commun.* **12**, 1 (2021).
- ²⁷J. Zhou, X. Shu, Y. Liu, X. Wang, W. Lin, S. Chen, L. Liu, Q. Xie, T. Hong, P. Yang, B. Yan, X. Han, and J. Chen, *Phys. Rev. B* **101**, 184403 (2020).
- ²⁸R. Shindou and N. Nagaosa, *Phys. Rev. Lett.* **87**, 116801 (2001).
- ²⁹J. Kübler and C. Felser, *EPL* **108**, 67001 (2014).
- ³⁰H. Chen, Q. Niu, and A. H. MacDonald, *Phys. Rev. Lett.* **112**, 017205 (2014).
- ³¹N. Nagaosa, J. Sinova, S. Onoda, A. H. MacDonald, and N. P. Ong, *Rev. Mod. Phys.* **82**, 1539 (2010).
- ³²T. Higo, D. Qu, Y. Li, C. Chien, Y. Otani, and S. Nakatsuji, *Appl. Phys. Lett.* **113**, 202402 (2018).
- ³³W. Han, Y. Otani, and S. Maekawa, *npj Quantum Mater.* **3**, 1 (2018).
- ³⁴J. Nogués and I. K. Schuller, *J. Magn. Magn. Mater.* **192**, 203 (1999).
- ³⁵Y.-W. Oh, S.-H. Chris Baek, Y. M. Kim, H. Y. Lee, K.-D. Lee, C.-G. Yang, E.-S. Park, K.-S. Lee, K.-W. Kim, G. Go, J.-R. Jeong, B.-C. Min, H.-W. Lee, K.-J. Lee, and B.-G. Park, *Nat. Nano.* **11**, 878 (2016).
- ³⁶S. Fukami, C. Zhang, S. DuttaGupta, A. Kurenkov, and H. Ohno, *Nat. Mater.* **15**, 535 (2016).
- ³⁷A. van den Brink, G. Vermeij, A. Solignac, J. Koo, J. T. Kohlhepp, H. J. Swagten, and B. Koopmans, *Nat. Commun.* **7**, 1 (2016).
- ³⁸A. Migliorini, B. Kuerbanjiang, T. Huminiuc, D. Kepaptsoglou, M. Muñoz, J. Cuiñado, J. Camarero, C. Aroca, G. Vallejo-Fernández, V. Lazarov, and J. Prieto, *Nat. Mater.* **17**, 28 (2018).
- ³⁹M. Tsunoda, K.-i. Imakita, M. Naka, and M. Takahashi, *J. Magn. Magn. Mater.* **304**, 55 (2006).
- ⁴⁰L. G. Parratt, *Phys. Rev.* **95**, 359 (1954).
- ⁴¹R. Bansal, N. Behera, A. Kumar, and P. Muduli, *Appl. Phys. Lett.* **110**, 202402 (2017).
- ⁴²E. V. Khomenko, N. G. Chechenin, A. Y. Goikhman, and A. V. Zenkevich, *JETP Lett.* **88**, 602 (2008).
- ⁴³A. Kumar, R. Sharma, K. I. Ali Khan, C. Murapaka, G. J. Lim, W. S. Lew, S. Chaudhary, and P. K. Muduli, *ACS Appl. Electron. Mater.* **3**, 3139 (2021).
- ⁴⁴L. Liu, T. Moriyama, D. C. Ralph, and R. A. Buhrman, *Phys. Rev. Lett.* **106**, 036601 (2011).
- ⁴⁵A. Bose, N. J. Schreiber, R. Jain, D.-F. Shao, H. P. Nair, J. Sun, X. S. Zhang, D. A. Muller, E. Y. Tsymbal, D. G. Schlom, and D. C. Ralph, *Nat. Electron.* **5**, 267 (2022).
- ⁴⁶C. Kittel, *Phys. Rev.* **73**, 155 (1948).
- ⁴⁷V. Tshitoyan, C. Ciccirelli, A. Mihai, M. Ali, A. Irvine, T. Moore, T. Jungwirth, and A. Ferguson, *Phys. Rev. B* **92**, 214406 (2015).
- ⁴⁸V. P. Amin, P. M. Haney, and M. D. Stiles, *J. Appl. Phys.* **128**, 151101 (2020).
- ⁴⁹M. B. Lifshits and M. I. Dyakonov, *Phys. Rev. Lett.* **103**, 186601 (2009).
- ⁵⁰B. K. Hazra, B. Pal, J.-C. Jeon, R. R. Neumann, B. Goebel, B. Grover, H. Deniz, A. Styervoyedov, H. Meyerheim, I. Mertig, S.-H. Yang, and S. S. P. Parkin, arXiv:2211.12398 (2022).
- ⁵¹H. Saglam, J. C. Rojas-Sanchez, S. Petit, M. Hehn, W. Zhang, J. E. Pearson, S. Mangin, and A. Hoffmann, *Phys. Rev. B* **98**, 094407 (2018).
- ⁵²J. Zhou, X. Wang, Y. Liu, J. Yu, H. Fu, L. Liu, S. Chen, J. Deng, W. Lin, X. Shu, H. Y. Yoong, T. Hong, M. Matsuda, P. Yang, S. Adams, B. Yan, X. Han, and J. Chen, *Sci. Adv.* **5**, eaau6696 (2019).

Supplemental Materials: Interfacial origin of unconventional spin-orbit torque in Py/ γ -IrMn₃

S-I. EFFECT OF CU THICKNESS ON INTERFACE BETWEEN PY AND γ -IRMN₃

A Cu spacer can control the exchange coupling in the Py/ γ -IrMn₃ thin films. We use the ferromagnetic resonance (FMR) method to determine the effect of Cu thickness at the Py/ γ -IrMn₃ interface. From FMR measurements, we determine the exchange bias of Py/ γ -IrMn₃ from the resonance fields (H_R) for the positive and negative fields. Figure S1(a) shows measured FMR spectra for Py/ γ -IrMn₃ and Py/Cu/ γ -IrMn₃ samples. The resonance field in Py/ γ -IrMn₃ is changed by reversing the field direction. This is caused by the exchange bias, which can be determined as $H_{ex} = |H_R(H > 0) - H_R(H < 0)|/2$. Figure S1(b) shows the behavior of H_{ex} with the thickness of the Cu spacer. The exchange bias shows a steep decrease with the thickness of the Cu layer. The exchange bias completely disappears after a thickness of 1 nm of Cu. Hence, we chose Py/Cu/IrMn₃ samples with 1.5 nm Cu in the main text to eliminate the exchange coupling between Py and γ -IrMn₃.

S-II. THICKNESS DEPENDENCE OF THE SOT EFFICIENCIES

SOT efficiency was measured for different thicknesses of Py in contact with γ -IrMn₃. Figure S2 (a), (d) shows the STFMR spectra for Py(5 nm)/ γ -IrMn₃ and Py(13 nm)/ γ -IrMn₃. The angular-dependent of V_S and V_A is shown in Fig. S2 (b), (c), (e), and (f) show the presence of unconventional torque in both systems. We summarize the extracted torques in Table S1. Though all samples with Py/ γ -IrMn₃ show the presence of USOT, no systematic thickness dependence is observed by varying Py thickness from 5 nm→8.7 nm→13 nm. We also found larger $\xi_{DL}^z > \xi_{DL}^y$ for all the samples.

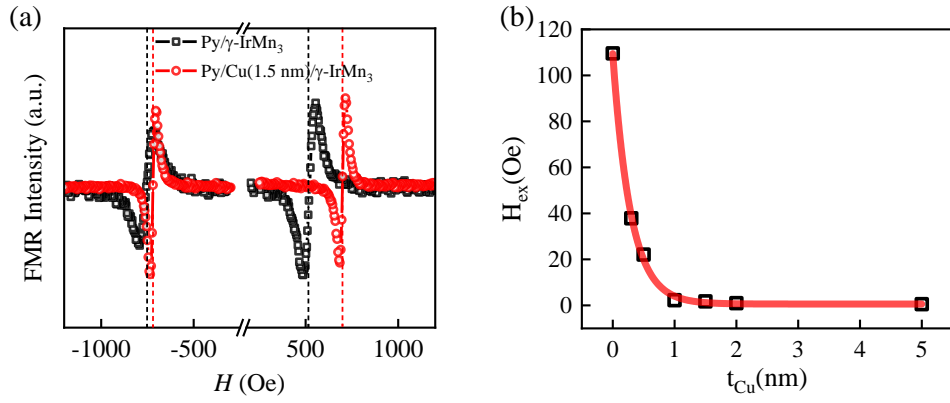


FIG. S1. (a) FMR measurements for Py/ γ -IrMn₃ (black) and Py/Cu (1.5 nm)/ γ -IrMn₃ (red) sample measured at 8 GHz with sweeping magnetic field parallel to exchange bias. The field reversal spectra show that exchange bias generates a shift in the resonance field in Py/ γ -IrMn₃. (b) Variation of exchange bias as a function of Cu spacer thickness.

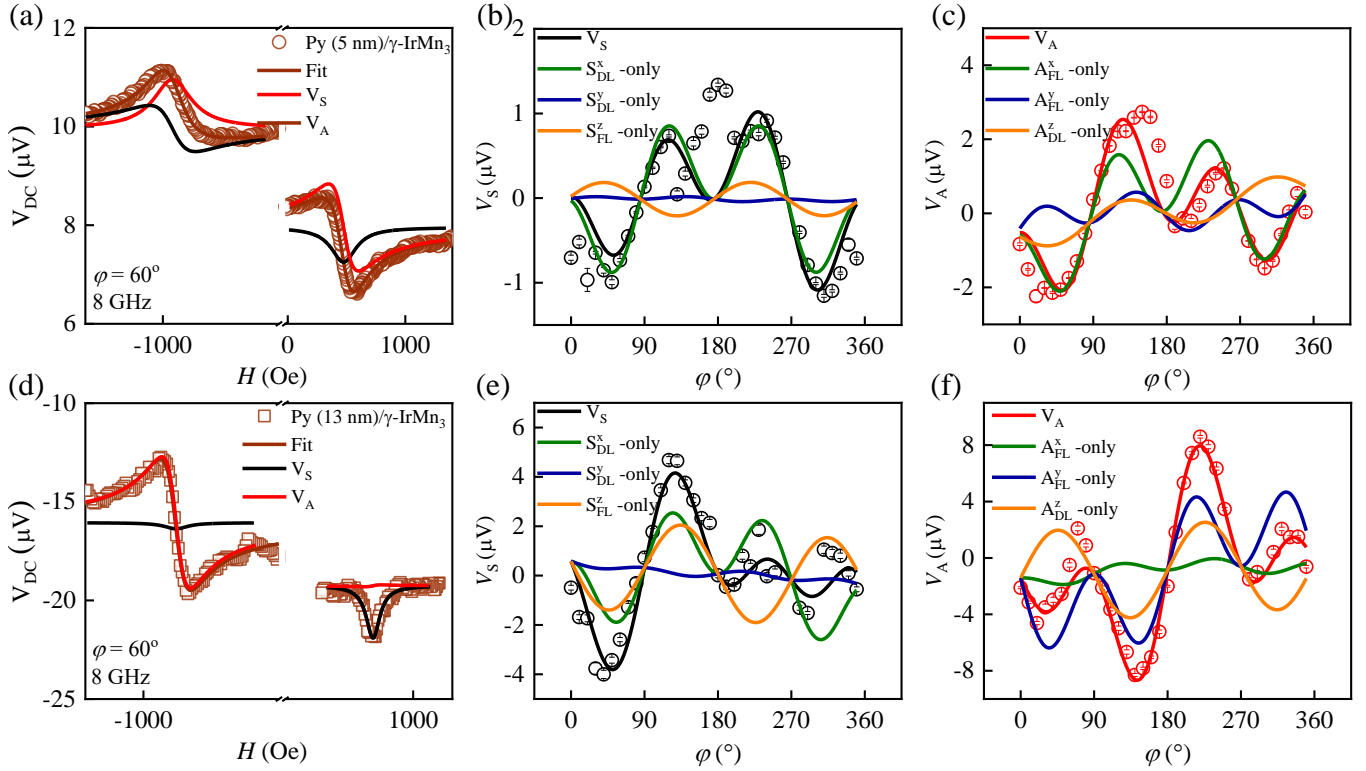


FIG. S2. STFM measurements on (a) Py(5 nm)/ γ -IrMn₃, and (d) Py(13 nm)/ γ -IrMn₃, Angular dependence of V_S and V_A components for (b), and (c) Py(5 nm)/ γ -IrMn₃, and (e), and (f) Py(13 nm)/ γ -IrMn₃. The solid lines in (a) and (d) represent Lorentzian fit using Eq (1) of the main text. The symmetric (V_S) and anti-symmetric (V_A) components of the fitted curve are depicted in black and red, respectively. The fitting (solid lines) in (b), (c), (e), and (f) are performed using Eq. (2) and Eq. (3) of the main text. The solid lines (brown, blue, and green) in these figures show the extracted angular dependence of voltage contributions from x -, y -, and z -direction spin polarization.

TABLE S1. Spin polarization direction and damping-like efficiency for different Py thickness:

Sample	Direction of polarization	Damping-like efficiency		
		ξ_{DL}^x	ξ_{DL}^y	ξ_{DL}^z
Py (5 nm)/ γ -IrMn ₃	x -, y -, and z - direction	-0.58 ± 0.19	0.02 ± 0.10	-0.06 ± 0.04
Py (13 nm)/ γ -IrMn ₃	x -, y -, and z - direction	0.53 ± 0.06	0.04 ± 0.08	-0.15 ± 0.02